SAND--89-0815C

DE89 013935

Proc. Soc. Experimental Mechanics
Spring 1989 Conference
Cambridge, Mass., May '89

THERMAL STRAINS IN A BIMATERIAL JOINT: EXPERIMENTAL AND NUMERICAL ANALYSIS

J. D. Wood, M. Y. Tsai, D. Post, J. Morton
Engineering Science and Mechanics Department
Virginia Polytechnic Institute and State University
Blacksburg, VA 24061

V. J. Parks
Civil Engineering Department
The Catholic University of America
Washington, DC 20064

F. P. Gerstle, Jr.
Sandia National Laboratories
Albuquerque, NM 87185

ABSTRACT

A comprehensive stress analysis was performed for a bimaterial plate subjected to a uniform change of temperature. The steel and brass portions of the specimen were bonded along a common edge. Whole-field measurements were made by high-sensitivity moire interferometry. A companion finite element numerical analysis of a similar body was conducted to help interpret the experimental results. The experiments documented a strong free-edge effect along the entire perimeter of the joint, an effect akin to a line singularity along the perimeter. High stresses in the edge-effected zone were determined from measurements, and enormous stress gradients were deduced by analysis. The largest stresses were found at the corner, where two edge-effected zones intersected.

INTRODUCTION

The complex state of elastic strains and stresses in a bimaterial joint subjected to a uniform change of temperature was investigated. The specimen configuration illustrated in Fig. 1 was studied. The steel and brass plates were joined by a thin, continuous, high-temperature silver-solder film along the mating surfaces.

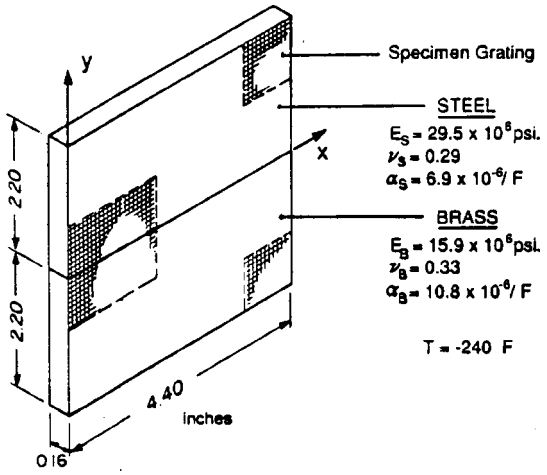

Fig. 1. Bimetal specimen with specimen gratings.

The experimental analysis utilized high-sensitivity moire interferometry with a specimen grating frequency of f = 2400 lines/mm, i.e., 60,960 lines/in. It was performed by the procedure reported in detail at the SEM Fall 1988 Conference in Indianapolis [1].

Briefly, the method consisted of heating the steel/brass plate to 310°F and replicating a uniform specimen grating on its surface at that temperature. Upon cooling to room temperature (70°F), the specimen and its grating deformed as a result of two parameters: (a) the free thermal contraction of the steel and brass and (b) the state of stress caused by the mutual constraint along the joint interface. This deformation was recorded (at room temperature) in a 4-beam moire interferometer [2]. The specimen gratings shown near the free (unstressed) corners in Fig. 1 experienced the same thermal cycle and they were used to determine experimentally the free thermal contraction and the thermal coefficient of expansion of each material. Carrier fringes of extension [3] were used to emphasize features of the deformation field. In addition, a special technique was applied whereby the carrier fringes cancelled the deformation fringes of free thermal contraction, leaving a pattern that represented the stress-induced displacements alone [1].

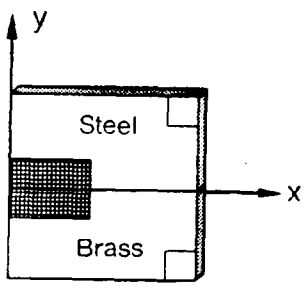

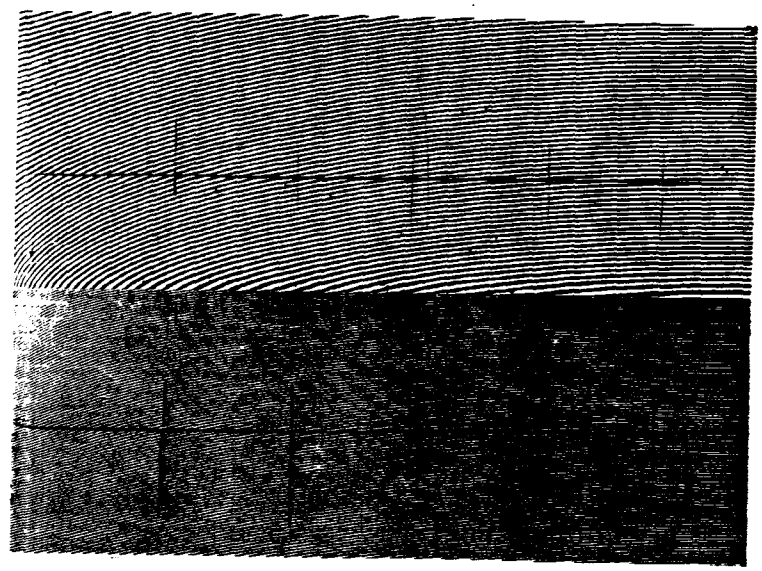

(a)

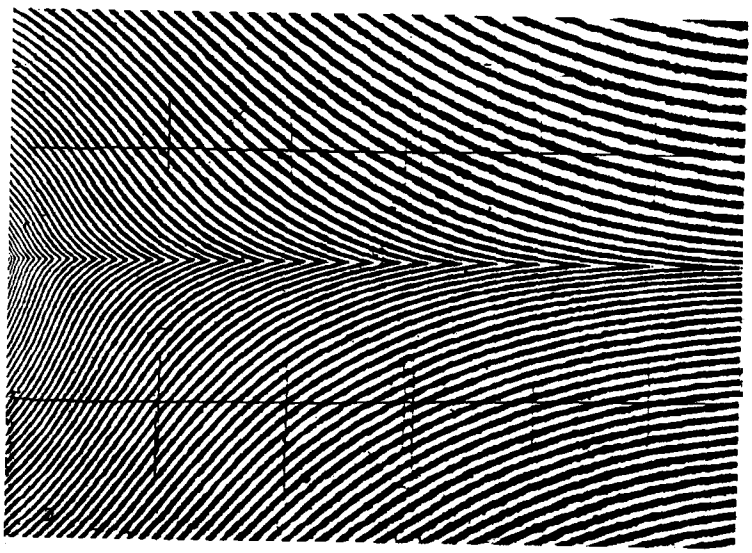

(b)

Fig. 2. V displacement fields in hatched region for $\Delta T = -240°F$. (a) contours of N_y^t, depicting the total displacements. (b) V field modified by carrier fringes of extension. (c) Contours of N_y^σ, depicting the stress-induced displacements in steel (top) and brass.

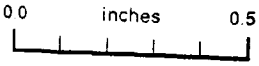

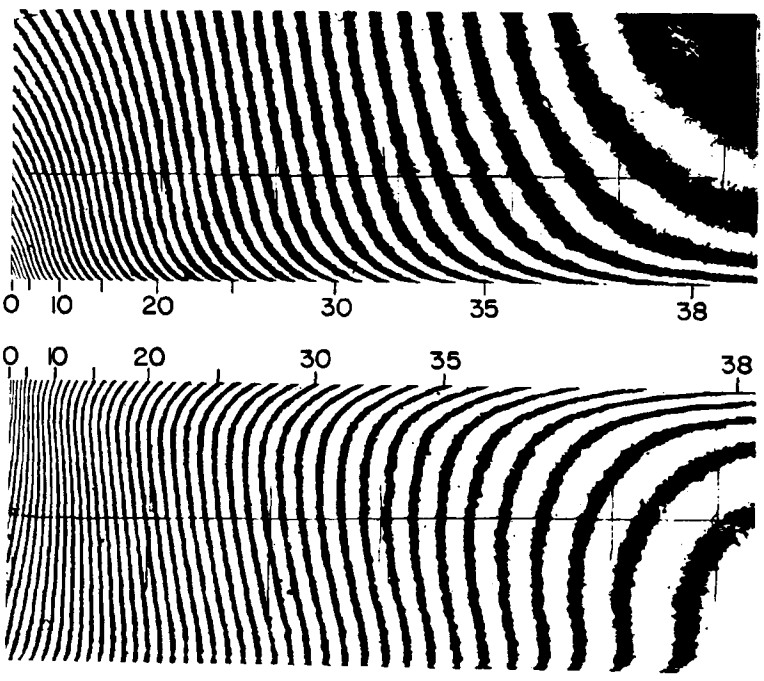

(c)

RELATIONSHIPS AND NOTATION

The following equations of moire interferometry and elastic thermal stress analysis were used to analyze the experimental results. The results are described in terms of the notation defined here.

$$U = \frac{1}{f} N_x^t \qquad V = \frac{1}{f} N_y^t \tag{1}$$

$$\varepsilon^t = \varepsilon^\sigma + \varepsilon^\alpha = \varepsilon^\sigma + \alpha\, \Delta T \tag{2}$$

$$\varepsilon_x^\sigma = \frac{\partial U}{\partial x} - \varepsilon^\alpha = \frac{1}{f}\frac{\partial N_x^t}{\partial x} - \varepsilon^\alpha = \frac{1}{f}\frac{\partial N_x^\sigma}{\partial x} \tag{3}$$

$$\varepsilon_y^\sigma = \frac{\partial V}{\partial y} - \varepsilon^\alpha = \frac{1}{f}\frac{\partial N_y^t}{\partial y} - \varepsilon^\alpha = \frac{1}{f}\frac{\partial N_y^\sigma}{\partial y} \tag{4}$$

$$\gamma_{xy}^\sigma = \frac{\partial U}{\partial y} + \frac{\partial V}{\partial x} = \frac{1}{f}\left(\frac{\partial N_x^t}{\partial y} + \frac{\partial N_y^t}{\partial x}\right) \tag{5}$$

$$\sigma_x = \frac{E}{1-\nu^2}\left(\varepsilon_x^\sigma + \nu\varepsilon_y^\sigma\right) \tag{6}$$

$$\sigma_y = \frac{E}{1-\nu^2}\left(\varepsilon_y^\sigma + \nu\varepsilon_x^\sigma\right) \tag{7}$$

$$\tau_{xy} = G\gamma_{xy} = \frac{E\,\gamma_{xy}}{2(1+\nu)} \tag{8}$$

where

U and V are the x and y components of displacement at a point;

N_x^t and N_y^t are fringe orders in the patterns of total displacements;

N_x^σ and N_y^σ are fringe orders in the patterns of stress-induced displacements;

f is 2400 lines/mm or 60,960 lines/in.;

ε and γ are normal and shear strains;

superscripts t, σ and α represent the total strain, the stress-induced part of the strain, and the free thermal expansion part of the strain;

α is coefficient of thermal expansion, listed in Fig. 1 for steel and brass;

ΔT is the temperature increment;

σ and τ are normal stress and shear stress;

E is modulus of elasticity, listed in Fig. 1;

ν is Poisson's ratio, listed in Fig. 1; and

G is shear modulus of elasticity (or modulus of rigidity).

Equations 2-4 and 6-8 pertain to the steel and brass portions separately, inasmuch as α, E and ν are different in the two materials. Shear stresses and shear strains are independent of uniform thermal contraction, so either N^t or N^σ can be used in Eq. 5.

RESULTS: MOIRE INTERFEROMETRY

The direct results of moire interferometry are shown in Figs. 2 and 3. Figure 2a is the total V displacement field, i.e., the N_y^t pattern. It is dominated by the thermal contraction of each part, steel and brass, thus the gradient $\partial N_y^t/\varepsilon_y$ is negative everywhere. Of course, the displacements are continuous across the steel/brass interface. The stress-induced deformations combine with the free thermal contractions to produce a sharp change of fringe gradient across the interface. This change is emphasized in Fig. 2b, where carrier fringes of extension were introduced. They have the effect of subtracting off a uniform strain equal to the average, approximately, of the thermal contractions. Clearly, the change across the interface is very abrupt. In the case of Fig. 2c, the carrier fringes produced a uniform apparent strain equal and opposite to ε^α (or $\alpha\Delta T$), which had the effect of cancelling the free thermal contraction part of the fringe pattern [1]. The result was the pattern of the stress-induced displacements -- the contour map of N_y^σ. The procedure was carried out separately for the upper and lower regions since the magnitudes of α are different for the steel and brass.

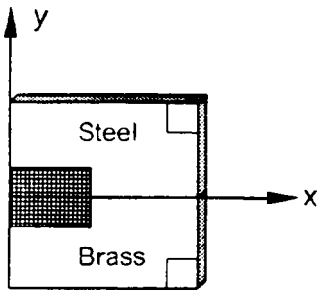

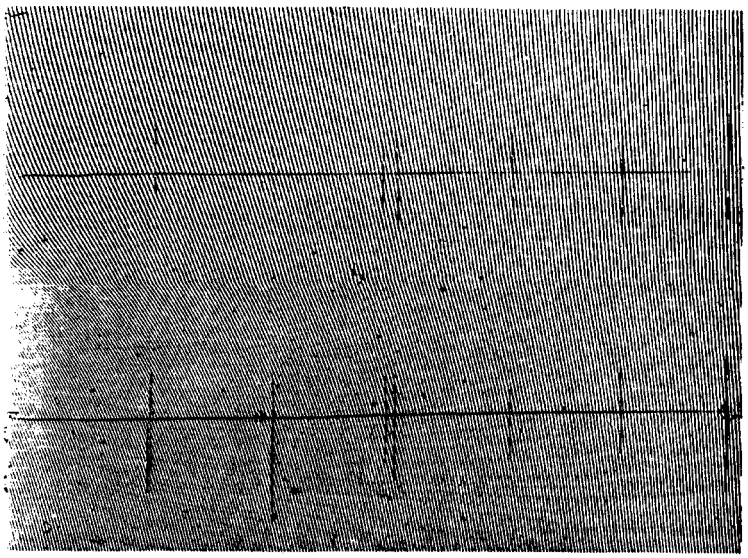

(a)

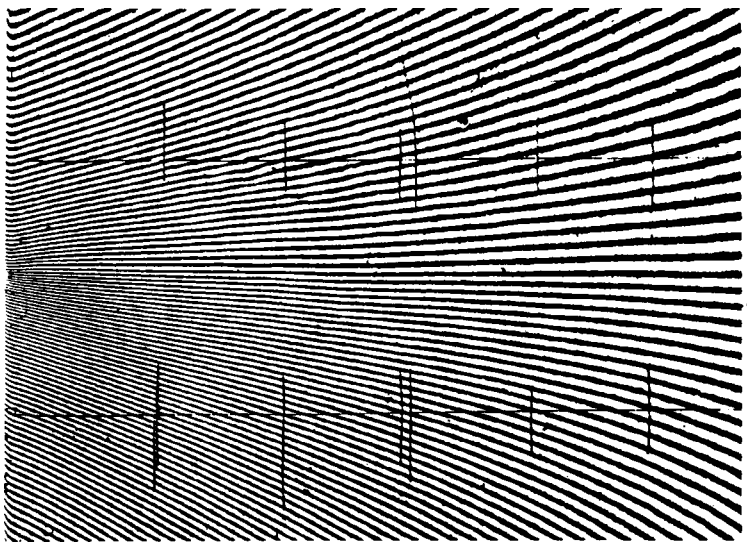

(b)

Fig. 3. U displacement fields for $\Delta T = -240°F$. (a) contours of N_x^t. (b) U field with carrier of extension. (c) Contours of N_x^σ.

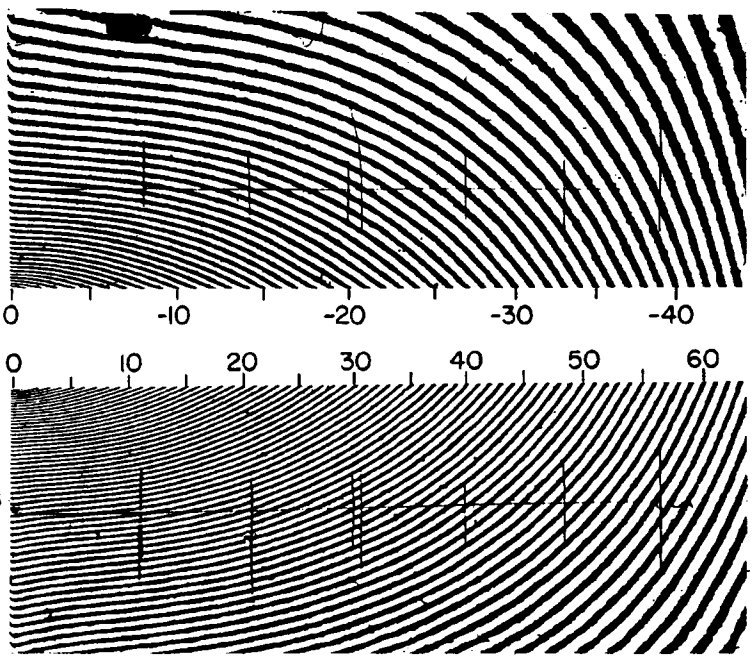

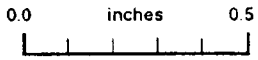

(c)

The corresponding U displacement fields are shown in Fig. 3, where (a) is the total displacement pattern of N_x^t fringes; (b) is the same field, but combined with a carrier that subtracts off a strain equal (approximately) to the average of the thermal contractions; and (c) is the stress-induced part of the U field, depicted by contours of N_x^σ. Pattern (b) proves that the ε_x^t strains in the steel and brass are constant along the interface and identical in the two materials. The fringe orders marked in (c) indicate that the stress-induced strain ε_x^σ along the interface is compressive in the steel and tensile in the brass. This is consistent with the greater thermal contraction of the brass and the opposing restraint by the steel.

RESULTS: MECHANICAL DIFFERENTIATION

Figure 4 introduces another kind of fringe pattern, the pattern of mechanical differentiation [2,4,5]. The pattern is constructed by superimposing two identical transparencies of Fig. 3a and shifting one relative to the other by a finite increment Δx. When shifted, the dark lines of the two patterns interweave and create a moire effect. The effect is known as geometric moire, as distinguished from the interferometric moire of Figs. 2 and 3. The fringes in Fig. 4 are contour lines of the finite increment approximation of $\partial U/\partial x$, contour lines of the normal strain ε_x. The relationship is approximate in the same sense that the finite element method of numerical analysis is approximate. Its accuracy is good only in regions where the strain gradient in the finite increment Δx is small. In this case, it provides meaningful data for most of the field.

An important feature of the strain distribution is the irregular nature of fringes in Fig. 4. A theoretical elasticity solution would show smooth contours, so the irregularities must be associated with the irregular nature of the real specimen. While one is tempted to blame this on gaps or cracks in the silver-solder joint, cracks would cause discontinuities in the fringes. Furthermore, some irregularities occur at substantial distances from the interface and they are not synchronized with those near the interface. We believe that there are no gaps or cracks in the joint, but instead, the material exhibits small irregularities of its mechanical properties. Variations of the thermal coefficients of expansion of the two materials is the primary suspect, and these variations might be heightened in a heat-effected zone near the silver-soldered interface. If the irregularities were caused by random variations of the coefficients of expansions, the fringes must be smoothed to represent stress-induced strains. Certain smoothing of data was done in the analysis.

RESULTS: GRAPHS

The displacement patterns of Figs. 2 and 3 were analyzed in accord with Eqs. 3-5. A detailed analysis was performed along the y' axis at the quarter-width of the specimen. The results for stress-induced strains are plotted in Fig. 5. Corresponding strains are substantially different in sign and magnitude for the steel and brass. The difference of strains ε_x^σ in steel and brass is equal to the difference of free thermal contractions. The ε_x^σ and γ_{xy} curves are nearly linear and data extraction from Figs. 2c and 3c was relatively easy. Special attention was given to the determination of the ε_y^σ curves and their values at the interface. These data were extracted from Fig. 2a by (a) measuring fringe positions on an enlarged pattern by means of a digitizing tablet, (b) calculating the incremental derivative $\Delta N_x^t/\Delta x$ between fringes, and (c) calculating the best fit of a second degree curve to the high-gradient portion of the data. Accuracy of the peak strains ε_y^σ is estimated to be within 0.5×10^{-4}.

The corresponding stresses were calculated from the strains by Eqs. 6-8; they are plotted in Fig. 6, where stress is given in thousands of pounds per square inch (ksi). The stress distributions are remarkably similar in the steel and brass. The shear stresses are nearly symmetrical and exhibit equal magnitudes at the interface. Normal stresses σ_x have similar distributions, but opposite signs. This difference between interface values does not violate equilibrium. Normal stresses σ_y exhibit nearly the same peak values in steel and brass and the distributions are almost the same, but with opposite signs. The apparent violation of σ_y equilibrium at the interface will be discussed later.

A detailed analysis of the fringe patterns, Figs. 2 and 3, was performed along the interface, too. The stresses are graphed in Fig. 7. They illustrate the remarkable result that the stress disturbance at the specimen corner is so highly localized -- within 0.05 inches of the corner or 1% of the specimen length for normal stresses and 0.15 inches for the shear stress. Elsewhere, the normal stresses are constant and the shear stresses change gradually along the interface length. Of course, these represent stresses at the surface of the specimen and they are not proposed as representative of the interior stresses along the interface. Further interpretation is reserved for the discussion section.

FINITE ELEMENT ANALYSIS

The experimental analysis led to the hypothesis that a strong free-edge effect exists along the interface near the free surface. To corroborate the hypothesis, it is necessary to determine internal stress distributions, which cannot be done by the experimental method. Instead, a related bimaterial thermal stress problem was investigated numerically by the finite element method.

Fig. 4. Contours of ε_x by mechanical differentiation

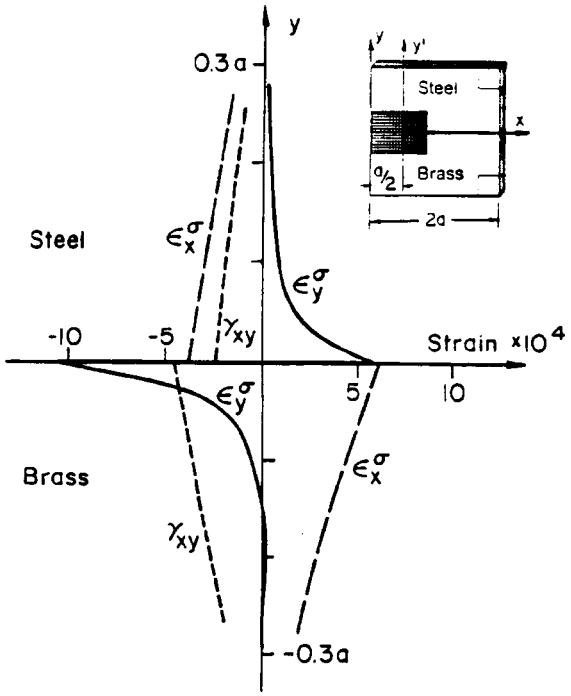

Fig. 5. The distribution of stress-induced strains on the y′ axis.

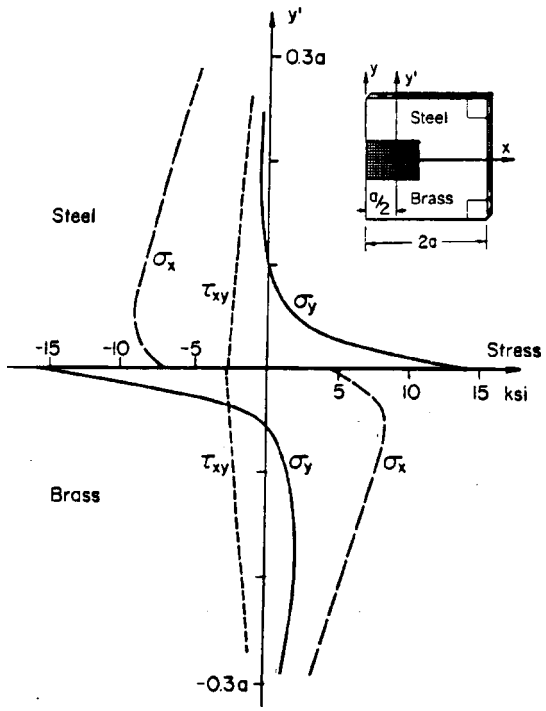

Fig. 6. The distribution of stresses on the y′ axis.

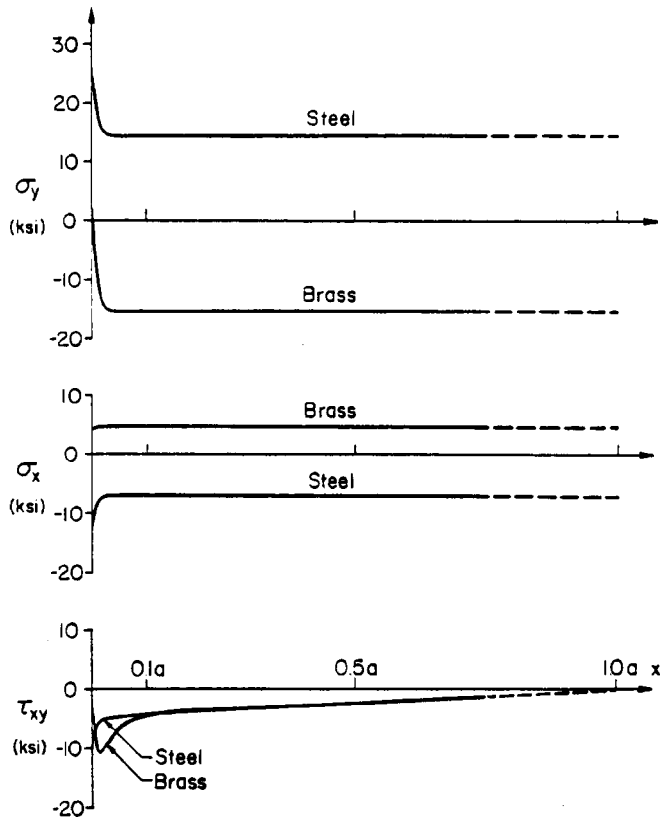

Fig. 7. The distribution of stresses from measurements along the interface.

The problem was that of two cylindrical solids with the elastic properties of steel and brass, joined together as illustrated in Fig. 8a and subjected to a -240°F temperature increment. An axially-symmetric geometry was selected to reduce the three-dimensional problem to a two-dimensional analysis, but nevertheless the results will test the hypothesis. The body was scaled such that its diameter-to-height ratio equalled the thickness-to-height ratio of the experimental specimen. Stresses in the radial (ry) plane were calculated using an extremely fine mesh in the region near the intersection of the interface and the free surface.

The calculated axial stresses, σ_y, along the free surface is plotted in Fig. 8b as a global view and in Fig. 8c as a highly magnified local view near the interface, with smaller scale increments by a factor of 100. It is interesting to note that the stresses fade to zero within one diameter of the interface. In the steel, σ_y increases as the interface is approached. In the brass, however, the σ_y curve reaches its peak negative value very close to the interface, but it reverses its course and rises as it approaches the interface more closely. The details are exhibited in (c). The ascent of the σ_y curve in the brass, through a stress increment of about 3000 psi, is well defined by numerous elements. In the shaded zone, the rise should not be taken to support the ascent since it is a zone in which the numerical model violates equilibrium. This violation is observed in the τ_{ry} values plotted in (c), which are known to be zero on the free surface. Thus, the points in the shaded zone are not dependable and they are not shown in (b). Nevertheless, the turnabout of the σ_y curve in the brass, and its ascent toward positive values, is dependably established by the finite element solution.

Numerical analyses with larger elements were conducted, too. A trend was established whereby progressively higher (dependable) σ_y values were calculated as the size of the elements decreased. This suggests that the elasticity solution with infinitesimal elements would yield a singularity solution of the form sketched in (d), in which the σ_y curve for the steel increases asymptotically while the curve for the brass reaches its minimum and then turns to rise asymptotically to approach a positive infinite value.

Figure 8e shows interior stresses acting in the radial ry plane along lines ± 0.025 R and ± 0.050 R from the interface. These lines are very close to the interface, but they are outside the hatched zone of graph (c). Of course, the values of σ_y at the free surface (r = R) matches those in (c) at corresponding y positions. Beneath the free surface, however, σ_y plunges toward zero stress in both the steel and brass. The strain gradients are extremely large. The companion stresses σ_r and τ_{ry} change rapidly with distance from the free surface and then very slowly along the radial lines. These results confirm the hypothesis -- they confirm the existence of a strong free-edge effect in a small volume of material near the perimeter of the interface. This edge-effected zone extends a small distance above and below the interface and a very small distance inwards from the interface. The zone is like a belt comprised of the material near the intersection of the interface with the free surface. Very high stresses and enormous stress gradients occur within this belt.

INTERPRETATION AND DISCUSSION

The results provide a rather comprehensive description of the deformation and the stresses distributed in the face of the bimaterial plate. An interpretation of special features is given here.

Figure 6 indicates a startling discontinuity of σ_y, suggesting a violation of equilibrium across the interface. The results of the FEM analysis indicate, however, that an enormous σ_y strain gradient exists near the interface. Accordingly, the stress curve for brass and/or steel experiences a very sharp turnaround and the two extreme values are connected by a shallow curve. This is accepted now as the interpretation of the experimental results. Thus, the σ_y stresses are single-valued at every point and equilibrium is not violated.

How is this interpretation rationalized with respect to the experimental data? The issue reduces to the interpretation of Fig. 2b. The fringes in the brass appear to exhibit decreasing slopes as they approach the interface. If the fringes have inflection points very close to the interface and curve in the opposite direction with increasing slopes, the fringe shape would be compatible with σ_y stress continuity across the interface. Such a transition could occur in a region so close to the interface that it would not be detected in the fringe pattern. Thus, the data does not preclude an enormous stress gradient and a shallow single-valued σ_y curve across the interface.

As illustrated in Fig. 7, the strongest stress disturbance occurs on the interface at the free corner, where two edge-effected zones intersect. The maximum tensile stress and the maximum shear stress are both about twice the respective values that occur away from the corner. The transition from the edge-effected zone to the corner-effected zone is abrupt and the corner-effected zone is highly localized.

If free-edge effects were absent, the only forces acting on the interface would be shear forces. These dominate the force distribution on each half of the body. Since the stresses on an elastic body depend only upon the forces and the body geometry, and since the dominant forces on the steel and brass parts are equal and opposite (i.e., the corresponding shear forces act in opposite directions on the two bodies), the stress distributions in the steel and brass should be basically the same, but of opposite signs. The experimental results shows a high degree of similarity of stress distributions in the steel and brass.

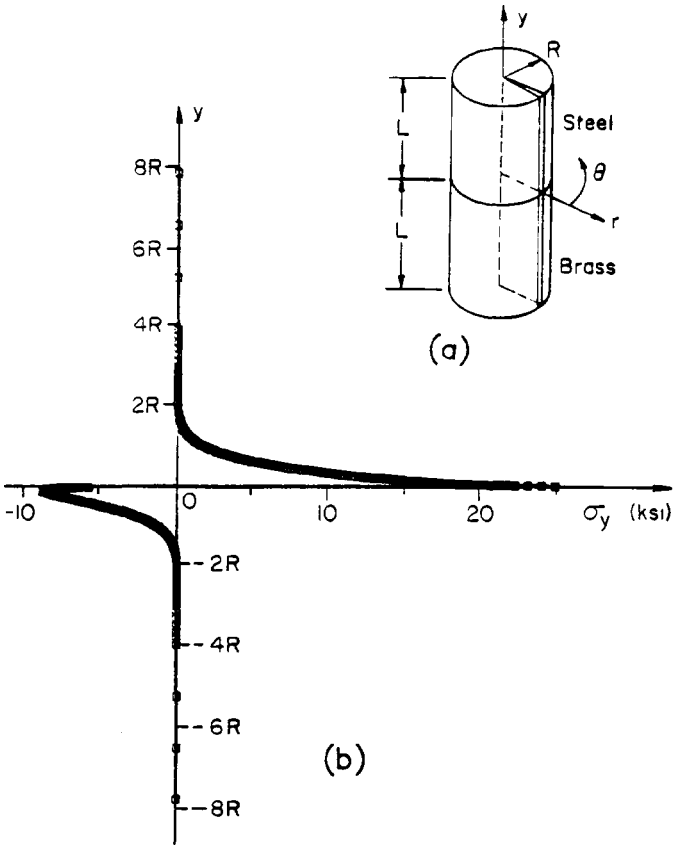

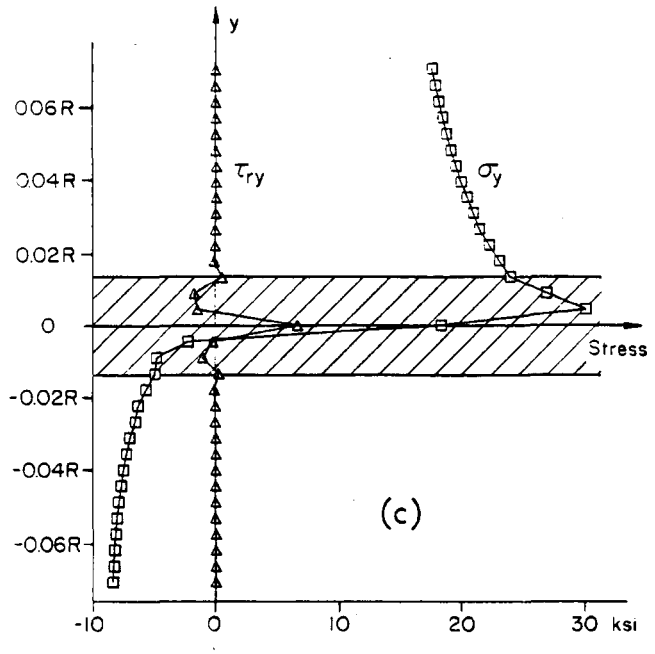

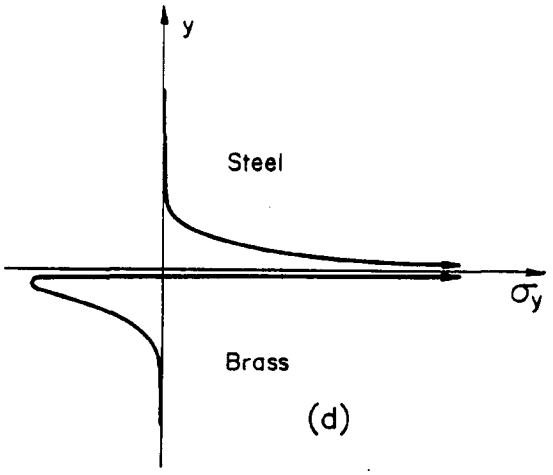

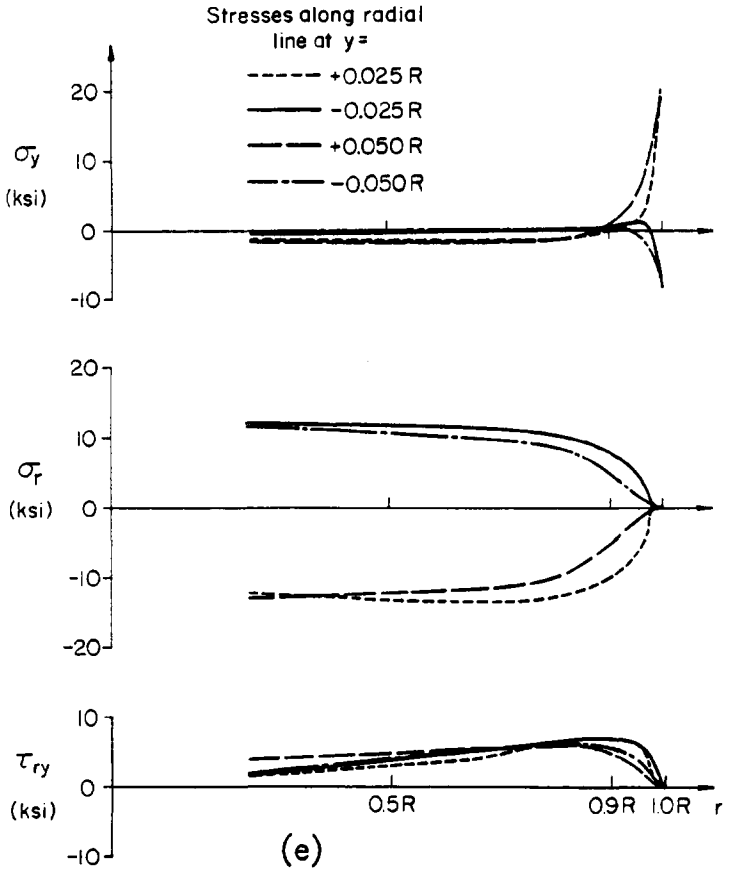

Fig. 8. Theoretical analysis by the finite element method. (a) The specimen of steel and brass. (b) σ_y vs. y across the interface. (c) Magnified view of (b). (d) Sketch of hypothetical singularity solution. (e) Interior stresses along radial lines at $y = \pm 0.025R$ and $\pm 0.050R$.

CONCLUSIONS

A comprehensive stress analysis of a bimaterial thermal stress problem was performed successfully by means of experimental measurements. A strong free-edge effect was documented along the perimeter of the joint. Large normal stresses were determined from deformation measurements, and enormous stress gradients in the interface region were deduced from this study.

An apparent violation of equilibrium was explained by a finite-element numerical analysis of a similar body. The enormous stress gradients found by the numerical study justified a stress continuity argument for the experimental results.

Stress variations in the edge-effected zone exhibited the same form as those in a theoretical three-dimensional singularity zone, except the stress magnitudes remained finite in the physical body. The bimaterial body can be viewed as a singularity problem in which a line singularity exists along the perimeter of the interface.

A localized but strong disturbance was observed in the corner region where two edge-effected zones intersected. Whole-field observations permitted the extraction of highly localized details while providing data for stress analysis of a large portion of the body.

ACKNOWLEGEMENTS

This work was sponsored by Sandia National Laboratories under Contract No. 75-8962 and by the National Center for Composite Materials Research under ONR Grant N00014-86-K0799. The support and encouragement are greatfully acnowledged.

gratefully

REFERENCES

[1] D. Post, and J. D. Wood, "Determination of Thermal Strains by Moire Interferometry," Proc. SEM Fall 1988 Conference, Indianapolis, IN (Nov. 1988).

[2] D. Post, "Moire Interferometry," Chap. 7, Handbook of Experimental Mechanics, A. S. Kobayashi, Ed., Prentice Hall, Englewood Cliffs, NJ (1987).

[3] Y. Guo, D. Post, and R. Czarnek, "The Magic of Carrier Fringes in Moire Interferometry," Experimental Mechanics, (to be published).

[4] J. P. Duncan and P. G. Sabin, "An Experimental Method for Recording Curvature Contours in Flexed Elastic Plates," Experimental Mechanics, 5(1), 22-28(1965).

[5] D. Post, R. Czarnek and D. Joh, " Shear-Strain Contours by Moire Interferometry," Experimental Mechanics, 25(1), 282-287 (Sept. 1985).

DISCLAIMER